

World Journal of *Gastrointestinal Oncology*

World J Gastrointest Oncol 2024 March 15; 16(3): 571-1090



EDITORIAL

- 571 Synchronous gastric and colon cancers: Important to consider hereditary syndromes and chronic inflammatory disease associations
Shenoy S
- 577 Neutrophil-to-lymphocyte ratio and platelet-to-lymphocyte ratio: Markers predicting immune-checkpoint inhibitor efficacy and immune-related adverse events
Jiang QY, Xue RY
- 583 Early-onset gastrointestinal cancer: An epidemiological reality with great significance and implications
Triantafyllidis JK, Georgiou K, Konstadoulakis MM, Papalois AE

REVIEW

- 598 Management of obstructed colorectal carcinoma in an emergency setting: An update
Pavlidis ET, Galanis IN, Pavlidis TE
- 614 Unraveling the enigma: A comprehensive review of solid pseudopapillary tumor of the pancreas
Xu YC, Fu DL, Yang F

MINIREVIEWS

- 630 Roles and application of exosomes in the development, diagnosis and treatment of gastric cancer
Guan XL, Guan XY, Zhang ZY
- 643 Prognostic and predictive role of immune microenvironment in colorectal cancer
Kuznetsova O, Fedyanin M, Zavalishina L, Moskvina L, Kuznetsova O, Lebedeva A, Tryakin A, Kireeva G, Borshchev G, Tjulandin S, Ignatova E
- 653 Pylorus-preserving gastrectomy for early gastric cancer
Sun KK, Wu YY

ORIGINAL ARTICLE**Case Control Study**

- 659 N-glycan biosignatures as a potential diagnostic biomarker for early-stage pancreatic cancer
Wen YR, Lin XW, Zhou YW, Xu L, Zhang JL, Chen CY, He J
- 670 Expression and significance of pigment epithelium-derived factor and vascular endothelial growth factor in colorectal adenoma and cancer
Yang Y, Wen W, Chen FL, Zhang YJ, Liu XC, Yang XY, Hu SS, Jiang Y, Yuan J

- 687 Impact of Alcian blue and periodic acid Schiff expression on the prognosis of gastric signet ring cell carcinoma

Lin J, Chen ZF, Guo GD, Chen X

Retrospective Cohort Study

- 699 Clinical profile and outcomes of hepatocellular carcinoma in primary Budd-Chiari syndrome

Agarwal A, Biswas S, Swaroop S, Aggarwal A, Agarwal A, Jain G, Elhence A, Vaidya A, Gupte A, Mohanka R, Kumar R, Mishra AK, Gamanagatti S, Paul SB, Acharya SK, Shukla A, Shalimar

- 716 Chinese herbal medicine decreases incidence of hepatocellular carcinoma in diabetes mellitus patients with regular insulin management

Lai HC, Cheng JC, Yip HT, Jeng LB, Huang ST

- 732 Combining systemic inflammatory response index and albumin fibrinogen ratio to predict early serious complications and prognosis after resectable gastric cancer

Ren JY, Wang D, Zhu LH, Liu S, Yu M, Cai H

- 750 Mucosa color and size may indicate malignant transformation of chicken skin mucosa-positive colorectal neoplastic polyps

Zhang YJ, Yuan MX, Wen W, Li F, Jian Y, Zhang CM, Yang Y, Chen FL

- 761 Epidemiology, therapy and outcome of hepatocellular carcinoma between 2010 and 2019 in Piedmont, Italy

Bracco C, Gallarate M, Badinella Martini M, Magnino C, D'Agnano S, Canta R, Racca G, Melchio R, Serraino C, Polla Mattiot V, Gollè G, Fenoglio L

- 773 Study on sex differences and potential clinical value of three-dimensional computerized tomography pelvimetry in rectal cancer patients

Zhou XC, Ke FY, Dhamija G, Chen H, Wang Q

Retrospective Study

- 787 High patatin like phospholipase domain containing 8 expression as a biomarker for poor prognosis of colorectal cancer

Zhou PY, Zhu DX, Chen YJ, Feng QY, Mao YH, Zhuang AB, Xu JM

- 798 Combining prognostic value of serum carbohydrate antigen 19-9 and tumor size reduction ratio in pancreatic ductal adenocarcinoma

Xia DQ, Zhou Y, Yang S, Li FF, Tian LY, Li YH, Xu HY, Xiao CZ, Wang W

- 810 Influence of transcatheter arterial embolization on symptom distress and fatigue in liver cancer patients

Yang XM, Yang XY, Wang XY, Gu YX

- 819 T2-weighted imaging-based radiomic-clinical machine learning model for predicting the differentiation of colorectal adenocarcinoma

Zheng HD, Huang QY, Huang QM, Ke XT, Ye K, Lin S, Xu JH

- 833 Predictive value of positive lymph node ratio in patients with locally advanced gastric remnant cancer

Zhuo M, Tian L, Han T, Liu TF, Lin XL, Xiao XY

- 844 Risk of cardiovascular death in patients with hepatocellular carcinoma based on the Fine-Gray model
Zhang YL, Liu ZR, Liu Z, Bai Y, Chi H, Chen DP, Zhang YM, Cui ZL
- 857 Preoperatively predicting vessels encapsulating tumor clusters in hepatocellular carcinoma: Machine learning model based on contrast-enhanced computed tomography
Zhang C, Zhong H, Zhao F, Ma ZY, Dai ZJ, Pang GD
- 875 Comparison of mismatch repair and immune checkpoint protein profile with histopathological parameters in pancreatic, periampullary/ampullary, and choledochal adenocarcinomas
Aydin AH, Turhan N
- 883 Assessment of programmed death-ligand 1 expression in primary tumors and paired lymph node metastases of gastric adenocarcinoma
Coimbra BC, Pereira MA, Cardili L, Alves VAF, de Mello ES, Ribeiro U Jr, Ramos MFKP

Observational Study

- 894 Identification of breath volatile organic compounds to distinguish pancreatic adenocarcinoma, pancreatic cystic neoplasm, and patients without pancreatic lesions
Tiankanon K, Pungpipattrakul N, Sukaram T, Chaiteerakij R, Rerknimitr R
- 907 Clinical features and prognostic factors of duodenal neuroendocrine tumours: A comparative study of ampullary and nonampullary regions
Fang S, Shi YP, Wang L, Han S, Shi YQ

Clinical and Translational Research

- 919 Construction of an immune-related gene signature for overall survival prediction and immune infiltration in gastric cancer
Ma XT, Liu X, Ou K, Yang L
- 933 Clinical efficacy and pathological outcomes of transanal endoscopic intersphincteric resection for low rectal cancer
Xu ZW, Zhu JT, Bai HY, Yu XJ, Hong QQ, You J
- 945 Identification of a novel inflammatory-related gene signature to evaluate the prognosis of gastric cancer patients
Hu JL, Huang MJ, Halina H, Qiao K, Wang ZY, Lu JJ, Yin CL, Gao F

Basic Study

- 968 Verteporfin fluorescence in antineoplastic-treated pancreatic cancer cells found concentrated in mitochondria
Zhang YQ, Liu QH, Liu L, Guo PY, Wang RZ, Ba ZC
- 979 Effects of *Helicobacter pylori* and Moluodan on the Wnt/ β -catenin signaling pathway in mice with precancerous gastric cancer lesions
Wang YM, Luo ZW, Shu YL, Zhou X, Wang LQ, Liang CH, Wu CQ, Li CP

- 991** Mitochondrial carrier homolog 2 increases malignant phenotype of human gastric epithelial cells and promotes proliferation, invasion, and migration of gastric cancer cells
Zhang JW, Huang LY, Li YN, Tian Y, Yu J, Wang XF
- 1006** Ubiquitin-specific protease 21 promotes tumorigenicity and stemness of colorectal cancer by deubiquitinating and stabilizing ZEB1
Lin JJ, Lu YC
- 1019** Long non-coding RNA GATA6-AS1 is mediated by N6-methyladenosine methylation and inhibits the proliferation and metastasis of gastric cancer
Shen JJ, Li MC, Tian SQ, Chen WM
- 1029** CALD1 facilitates epithelial-mesenchymal transition progression in gastric cancer cells by modulating the PI3K-Akt pathway
Ma WQ, Miao MC, Ding PA, Tan BB, Liu WB, Guo S, Er LM, Zhang ZD, Zhao Q

META-ANALYSIS

- 1046** Efficacy and safety of perioperative therapy for locally resectable gastric cancer: A network meta-analysis of randomized clinical trials
Kuang ZY, Sun QH, Cao LC, Ma XY, Wang JX, Liu KX, Li J

SCIENTOMETRICS

- 1059** Insights into the history and tendency of glycosylation and digestive system tumor: A bibliometric-based visual analysis
Jiang J, Luo Z, Zhang RC, Wang YL, Zhang J, Duan MY, Qiu ZJ, Huang C

CASE REPORT

- 1076** Managing end-stage carcinoid heart disease: A case report and literature review
Bulj N, Tomasic V, Cigrovski Berkovic M
- 1084** Hemorrhagic cystitis in gastric cancer after nanoparticle albumin-bound paclitaxel: A case report
Zhang XJ, Lou J

ABOUT COVER

Peer Review of *World Journal of Gastrointestinal Oncology*, Noha Elkady, MD, Assistant Professor, Department of Pathology, Faculty of Medicine Menoufia University, Shibin Elkom 32511, Egypt. drnohaelkady@gmail.com

AIMS AND SCOPE

The primary aim of *World Journal of Gastrointestinal Oncology* (*WJGO*, *World J Gastrointest Oncol*) is to provide scholars and readers from various fields of gastrointestinal oncology with a platform to publish high-quality basic and clinical research articles and communicate their research findings online.

WJGO mainly publishes articles reporting research results and findings obtained in the field of gastrointestinal oncology and covering a wide range of topics including liver cell adenoma, gastric neoplasms, appendiceal neoplasms, biliary tract neoplasms, hepatocellular carcinoma, pancreatic carcinoma, cecal neoplasms, colonic neoplasms, colorectal neoplasms, duodenal neoplasms, esophageal neoplasms, gallbladder neoplasms, *etc.*

INDEXING/ABSTRACTING

The *WJGO* is now abstracted and indexed in PubMed, PubMed Central, Science Citation Index Expanded (SCIE, also known as SciSearch®), Journal Citation Reports/Science Edition, Scopus, Reference Citation Analysis, China Science and Technology Journal Database, and Superstar Journals Database. The 2023 edition of Journal Citation Reports® cites the 2022 impact factor (IF) for *WJGO* as 3.0; IF without journal self cites: 2.9; 5-year IF: 3.0; Journal Citation Indicator: 0.49; Ranking: 157 among 241 journals in oncology; Quartile category: Q3; Ranking: 58 among 93 journals in gastroenterology and hepatology; and Quartile category: Q3. The *WJGO*'s CiteScore for 2022 is 4.1 and Scopus CiteScore rank 2022: Gastroenterology is 71/149; Oncology is 197/366.

RESPONSIBLE EDITORS FOR THIS ISSUE

Production Editor: Xiang-Di Zhang; Production Department Director: Xiang Li; Editorial Office Director: Jia-Ru Fan.

NAME OF JOURNAL

World Journal of Gastrointestinal Oncology

ISSN

ISSN 1948-5204 (online)

LAUNCH DATE

February 15, 2009

FREQUENCY

Monthly

EDITORS-IN-CHIEF

Monjur Ahmed, Florin Burada

EDITORIAL BOARD MEMBERS

<https://www.wjgnet.com/1948-5204/editorialboard.htm>

PUBLICATION DATE

March 15, 2024

COPYRIGHT

© 2024 Baishideng Publishing Group Inc

INSTRUCTIONS TO AUTHORS

<https://www.wjgnet.com/bpg/gerinfo/204>

GUIDELINES FOR ETHICS DOCUMENTS

<https://www.wjgnet.com/bpg/GerInfo/287>

GUIDELINES FOR NON-NATIVE SPEAKERS OF ENGLISH

<https://www.wjgnet.com/bpg/gerinfo/240>

PUBLICATION ETHICS

<https://www.wjgnet.com/bpg/GerInfo/288>

PUBLICATION MISCONDUCT

<https://www.wjgnet.com/bpg/gerinfo/208>

ARTICLE PROCESSING CHARGE

<https://www.wjgnet.com/bpg/gerinfo/242>

STEPS FOR SUBMITTING MANUSCRIPTS

<https://www.wjgnet.com/bpg/GerInfo/239>

ONLINE SUBMISSION

<https://www.f6publishing.com>



Retrospective Study

Preoperatively predicting vessels encapsulating tumor clusters in hepatocellular carcinoma: Machine learning model based on contrast-enhanced computed tomography

Chao Zhang, Hai Zhong, Fang Zhao, Zhen-Yu Ma, Zheng-Jun Dai, Guo-Dong Pang

Specialty type: Oncology

Provenance and peer review:

Unsolicited article; Externally peer reviewed.

Peer-review model: Single blind

Peer-review report's scientific quality classification

Grade A (Excellent): 0

Grade B (Very good): 0

Grade C (Good): C

Grade D (Fair): 0

Grade E (Poor): 0

P-Reviewer: Ozdemir HI, Turkey

Received: October 30, 2023

Peer-review started: October 30, 2023

First decision: December 21, 2023

Revised: December 26, 2023

Accepted: January 29, 2024

Article in press: January 29, 2024

Published online: March 15, 2024



Chao Zhang, Hai Zhong, Guo-Dong Pang, Department of Radiology, The Second Hospital of Shandong University, Jinan 250033, Shandong Province, China

Fang Zhao, Department of Radiology, Qilu Hospital of Shandong University, Jinan 250014, Shandong Province, China

Zhen-Yu Ma, Department of Radiology, Linglong Yingcheng Hospital, Yantai 265499, Shandong Province, China

Zheng-Jun Dai, Department of Scientific Research, Huiying Medical Technology Co., Ltd, Beijing 100192, China

Corresponding author: Guo-Dong Pang, MD, PhD, Associate Chief Physician, Doctor, Department of Radiology, The Second Hospital of Shandong University, No. 247 Beiyuan Road, Tianqiao District, Jinan 250033, Shandong Province, China. pgd226@aliyun.com

Abstract

BACKGROUND

Recently, vessels encapsulating tumor clusters (VETC) was considered as a distinct pattern of tumor vascularization which can primarily facilitate the entry of the whole tumor cluster into the bloodstream in an invasion independent manner, and was regarded as an independent risk factor for poor prognosis in hepatocellular carcinoma (HCC).

AIM

To develop and validate a preoperative nomogram using contrast-enhanced computed tomography (CECT) to predict the presence of VETC+ in HCC.

METHODS

We retrospectively evaluated 190 patients with pathologically confirmed HCC who underwent CECT scanning and immunochemical staining for cluster of differentiation 34 at two medical centers. Radiomics analysis was conducted on intratumoral and peritumoral regions in the portal vein phase. Radiomics features, essential for identifying VETC+ HCC, were extracted and utilized to develop a radiomics model using machine learning algorithms in the training set. The model's performance was validated on two separate test sets. Receiver

operating characteristic (ROC) analysis was employed to compare the identified performance of three models in predicting the VETC status of HCC on both training and test sets. The most predictive model was then used to construct a radiomics nomogram that integrated the independent clinical-radiological features. ROC and decision curve analysis were used to assess the performance characteristics of the clinical-radiological features, the radiomics features and the radiomics nomogram.

RESULTS

The study included 190 individuals from two independent centers, with the majority being male (81%) and a median age of 57 years (interquartile range: 51-66). The area under the curve (AUC) for the combined radiomics features selected from the intratumoral and peritumoral areas were 0.825, 0.788, and 0.680 in the training set and the two test sets. A total of 13 features were selected to construct the Rad-score. The nomogram, combining clinical-radiological and combined radiomics features could accurately predict VETC+ in all three sets, with AUC values of 0.859, 0.848 and 0.757. Decision curve analysis revealed that the radiomics nomogram was more clinically useful than both the clinical-radiological feature and the combined radiomics models.

CONCLUSION

This study demonstrates the potential utility of a CECT-based radiomics nomogram, incorporating clinical-radiological features and combined radiomics features, in the identification of VETC+ HCC.

Key Words: Hepatocellular carcinoma; Vessels encapsulating tumor clusters; Intratumoral and peritumoral regions; Radiomics features; Nomogram

©The Author(s) 2024. Published by Baishideng Publishing Group Inc. All rights reserved.

Core Tip: Vessels encapsulating tumor clusters (VETC) is an independent risk factor for poor prognosis in hepatocellular carcinoma (HCC) and currently determined only on histologic examination after surgical resection. We evaluated 190 patients with pathologically confirmed HCC and constructed a machine learning-based contrast-enhanced computed tomography radiomics model, performed canonical screening of features and multiple validations, and confirmed robustness on various data resources. The radiomics model showed remarkable performance in predicting the VETC subtype, and the results were reproducible, demonstrating that the approach may be applied to other patient samples. Radiomics could provide valuable information for assisting clinicians in pretreatment decision-making.

Citation: Zhang C, Zhong H, Zhao F, Ma ZY, Dai ZJ, Pang GD. Preoperatively predicting vessels encapsulating tumor clusters in hepatocellular carcinoma: Machine learning model based on contrast-enhanced computed tomography. *World J Gastrointest Oncol* 2024; 16(3): 857-874

URL: <https://www.wjgnet.com/1948-5204/full/v16/i3/857.htm>

DOI: <https://dx.doi.org/10.4251/wjgo.v16.i3.857>

INTRODUCTION

Hepatocellular carcinoma (HCC) is the fifth most frequently diagnosed cancer and the third cause of cancer-related mortality worldwide[1,2]. HCC accounts for 75%-90% of primary liver cancers and constitutes a major global health problem[3]; moreover, HCC is difficult to treat. As therapeutic strategies, liver transplantation (LT) and surgical resection remain the effective modalities for HCC. However, the long-term outcomes of patients after curative resection show marked diversity, which remains a substantial challenge in clinical management. The 5-year recurrence rate was more than 50%, even up to 70%[4], vs 25%-35% with LT[5]. Early metastasis is responsible for frequent relapse and high mortality of HCC[6].

As a typical solid tumor, angiogenesis of HCC is closely related to recurrence and metastasis. The sinusoidal structure of the tumor vasculature in HCC increases the propensity for blood-borne metastases to neighboring or distant sites[7,8]. The epithelial-mesenchymal transition (EMT) has been considered a key pattern in migration and invasion of HCC[9]. Recently, Fang *et al*[6] for the first time further emphasized this distinct pattern of tumor vascularization that is independent of EMT, which was characterized by the presence of cluster of differentiation 34 (CD34)+ vessels encapsulating tumor clusters (VETC) in pathological imaging. The VETC pattern plays a crucial role in enabling the entire tumor cluster to enter the bloodstream independently of invasion in HCC[10]. Several reports have shown that VETC is an independent risk factor for poor prognosis in HCC, and patients with VETC+ HCC show shorter overall survival and disease free survival and are more prone to progression and metastasis relative to patients with VETC- HCC[6,11,12]. In addition, Fang *et al*[13] indicated that the VETC pattern acts as a predictor of sorafenib benefit in patients with HCC. However, VETC is currently only determined only on histologic examination after surgical resection[14]. Therefore, preoperative diagnosis of VETC status in HCC is of great significance to help predict patient outcomes and decide on

therapeutic strategies in HCC.

Radiomics presents a noninvasive methodology and holds significant potential in terms of sensitivity, selectivity, and experimental viability for the diagnosis of diseases, staging tumors, and predicting prognosis[15,16]. Radiomics has found use in HCC, including preoperative prediction of pathological indicators[17], differential diagnosis[18], evaluating curative effect, and prognosis prediction[19]. Recently, Yu *et al*[20] applied gadolinium-ethoxybenzyl-diethylenetriamine pentaacetic acid-enhanced magnetic resonance imaging (MRI) radiomics approach to evaluate VETC in HCC, Dong *et al* [21] attempted to develop deep learning radiomics model of dynamic contrast-enhanced MRI to predict VETC in HCC. As a routine examination method, the emergence of computed tomography (CT) has made a qualitative leap in the imaging diagnosis of liver cancer and driven the progress of liver surgery. CT images are clear and stable, and are used for routine diagnosis and follow-up examination of liver cancer after rehabilitation. We hypothesized that radiomics features based on contrast-enhanced CT (CECT) scans might provide a preoperative reference for accurate prediction of VETC status in patients with HCC. To our knowledge, no studies have determined whether CECT-based radiomics features can be used to predict VETC status with HCC patients. The objective of this study was to develop and validate a nomogram based on clinical-radiological and radiomics features from intratumoral and peritumoral regions for preoperative prediction of VETC+ HCC using data from a multicenter study.

MATERIALS AND METHODS

Study patients

We retrospectively included consecutive patients who received a histological diagnosis of HCC between January 2017 and March 2023 for radiomics model construction, using two sample data sets from two separate hospitals: A training set and an internal test set from the Second Hospital of Shandong University (center 1), and an external test set from the Qilu Hospital of Shandong University (center 2). The institutional review board of the two centers approved this retrospective multicenter study and the requirement for informed consent was waived because of the retrospective data sets, IRB No. KYLL-2023LW044.

The inclusion criteria were as follows: (1) CECT in the liver was performed within 1 wk before surgery or biopsy; (2) Testing of the CD34 level by immunohistochemistry (IHC); (3) If there were multiple lesions, we selected the largest one and included its corresponding immunohistochemical diagnosis in the study; and (4) Complete clinical data. The exclusion criteria were as follows: (1) Patients who had undergone prior treatments, including anti-tumor therapies, radiofrequency ablation, transcatheter arterial chemoembolization, and other similar procedures; (2) Images with noticeable artifacts affecting the imaging analysis; and (3) Massive necrosis (a significant area of necrosis in HCC, with few solid components present).

Radcloud platform (version 7.2; Huiying Medical Technology Co., Ltd, Beijing, China) was used to manage the imaging data and conduct subsequent analysis of radiomics statistics. Finally, a total of 153 patients with HCC (121 men and 32 women; 76 VETC+ and 77 VETC-) from center 1 were enrolled into a training set and an internal test set. To ensure appropriate sample distribution, the dataset was randomly split into a training set and an internal test set using a ratio of 7:3 and a random seed of 39. Another cohort of 37 patients with HCC (32 men and 5 women; 18 VETC+ and 19 VETC-) from center 2 were enrolled into an external test set. For a visual representation of the patient recruitment process, please refer to [Figure 1](#).

VETC measurement

The VETC pattern of all 190 patients in this study was determined by IHC performed on surgical histopathology samples. A 7-point baseline sampling protocol was applied to sample specimens to measure HCC[22]. The definition of the VETC pattern is the presence of vessels that form cobweb-like networks and that encapsulate and separate individual tumor clusters an explicit and continuous lining of CD34-positive endothelium[12]. Under light microscopy (100 ×), the five most intensely vascularized fields were selected, and the total number of individual tumor clusters that were completely surrounded by endothelium was evaluated. The index of VETC was presented by the average number of encapsulated tumor clusters per field[6]. According to previous studies, cases with VETC index $\geq 5\%$ in whole or part of the HCC section by CD34 immunostaining were identified as VETC+, and those with VETC index $< 5\%$ were identified as VETC-[23]. Two experienced pathologists, each with over 10 years of experience, conducted a qualitative and independent pathological assessment. Both the pathologists were blinded to the clinical, laboratory, and imaging results of the CECT. In cases where there was disagreement, a third pathologist was consulted, and the matter was discussed until a consensus was reached.

CT examination

Contrast-enhanced liver CT was performed using a 256-section (GE Revolution; both GE Healthcare) or a 128-section (Siemens Somatom Definition; Siemens) multidetector CT scanner. The following CT acquisition parameters were used: Tube voltage 120 kVp, tube current 240 mAs, rotation time 0.5 s, matrix size 512 × 512, slice thickness 5 mm. Nonionic contrast agent (300 mg of iodine per milliliter, 3 mL/s, 1.5 mL/kg body weight, Omnipaque, GE Healthcare) was administered as a bolus rapidly *via* the antecubital vein using a syringe pump. The arterial phase (AP), portal vein phase, and delayed phase images were obtained during suspended respiration at 15 s, 30 s, and 180 s respectively.

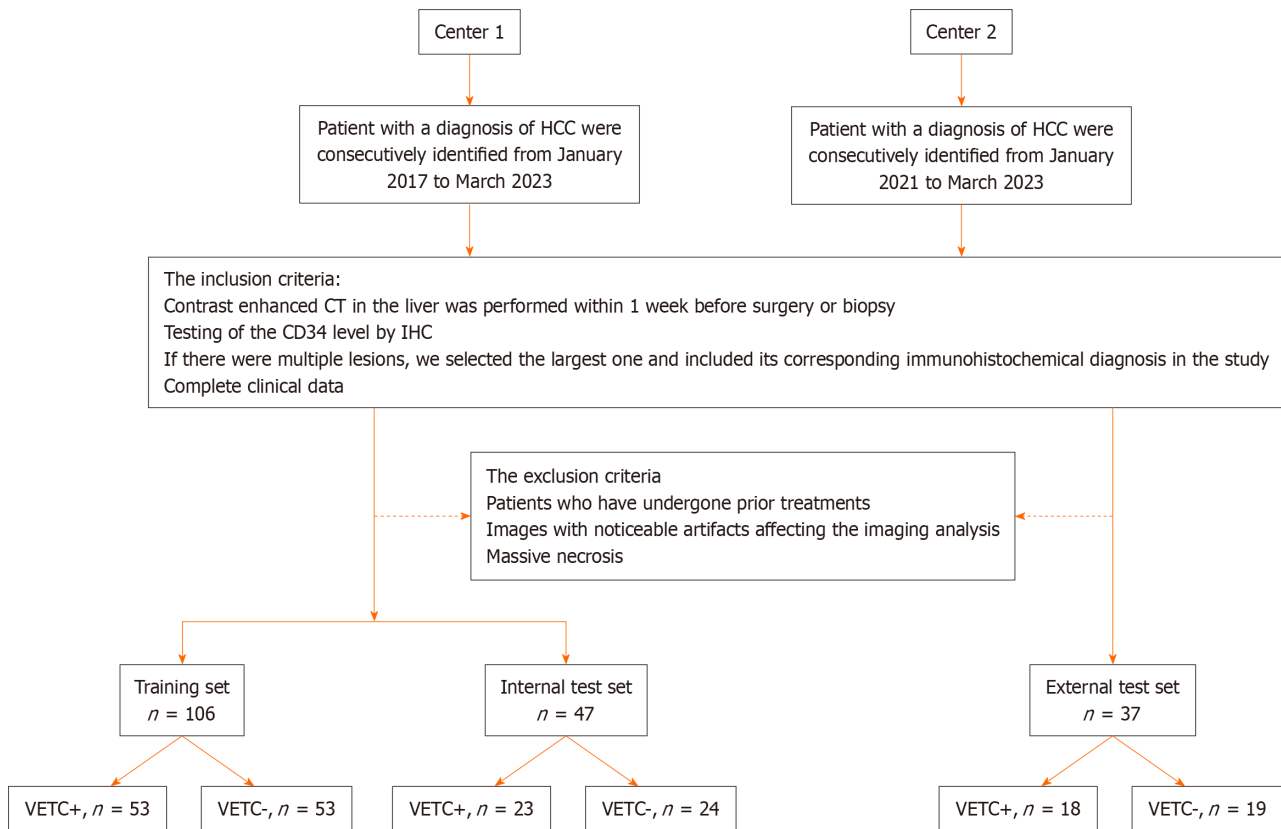


Figure 1 Flow chart of patient recruitment pathway. HCC: Hepatocellular carcinoma; CT: Computed tomography; IHC: Immunohistochemistry; VETC: Vessels encapsulating tumor clusters; CD34: Cluster of differentiation 34.

Image segmentation and radiomics feature extraction

The Radcloud platform was used for image segmentation purposes. Two radiologists (reader 1, 8 years of liver imaging experience; reader 2, 10 years of liver imaging experience) who were blinded to the clinical and histopathologic data delineated in a slice-by-slice manner the volumes of interest (VOI) of HCC from the portal venous phase images to obtain a tumor segmentation[24]. When there was a disagreement between the two radiologists, a senior radiologist (reader 3, 15 years of liver imaging experience) was consulted. Figure 2 provides an illustrative example of the tumor segmentation achieved through this process. To account for the peritumoral region, a topology algorithm was employed to dilate the region by a radius of 10 mm, as illustrated in Figure 2. In instances where the VOI extended beyond the liver parenchyma after the dilation, manual removal of the excessive portion was performed.

Following the segmentation of VOI-1 from intratumoral regions and VOI-2 from peritumoral regions, radiomics features were extracted using the Radcloud platform. Subsequently, a total of 3376 quantitative imaging features were extracted, including first-order statistics, 3D shape features, gray-level co-occurrence matrix features, gray-level run length matrix features, gray-level size zone matrix features, neighboring gray tone difference matrix features, and gray-level dependence matrix features. Notably, although shape features were solely derived from the original images, the remaining features could also be extracted after applying various filters such as wavelet, square, square root, gradient, logarithm, exponential, local binary pattern in 2D (lbp-2D), and lbp-3D. To obtain textural features, the preprocessed CT images underwent wavelet filtering. This involved the use of a built-in stationary wavelet transform employing high or low-pass filters in the X-, Y-, and Z- directions. Moreover, the lbp-3D image type consisted of three subcategories. One of these subcategories was the kurtosis map (lbp-3D-k), whereas the other two were calculated using varying levels of spherical harmonics, namely lbp-3D-m1 and lbp-3D-m2. All these radiomics features adhered to the image biomarker standardization initiative[25]. In addition, the values of these radiomics features were normalized using the z-score method.

Dimension reduction techniques were used to select relevant features and mitigate potential issues such as overfitting and bias during construction of the radiomics signature using the training set data. The workflow for the radiomics analysis is visually depicted in Figure 2. To assess interobserver reproducibility, two radiologists (reader 1 and reader 2) independently repeated the segmentation process on 30 randomly selected lesions after a one-month interval. The radiomics features demonstrating good agreement [interclass correlation coefficient (ICC) > 0.8] between the two readers were included in subsequent analyses. Moreover, a variance threshold of 0.8 was applied to further refine the feature selection process. Subsequently, SelectKBest, a univariate analysis method, was used to select features with *P* values less than 0.05 for further analysis. Finally, the optimal feature subset was constructed using the least absolute shrinkage and selection operator (LASSO). Regularization parameter (alpha) tuning was performed through 10-fold cross-validation, and features with non-zero coefficients were selected for subsequent radiomics analysis.

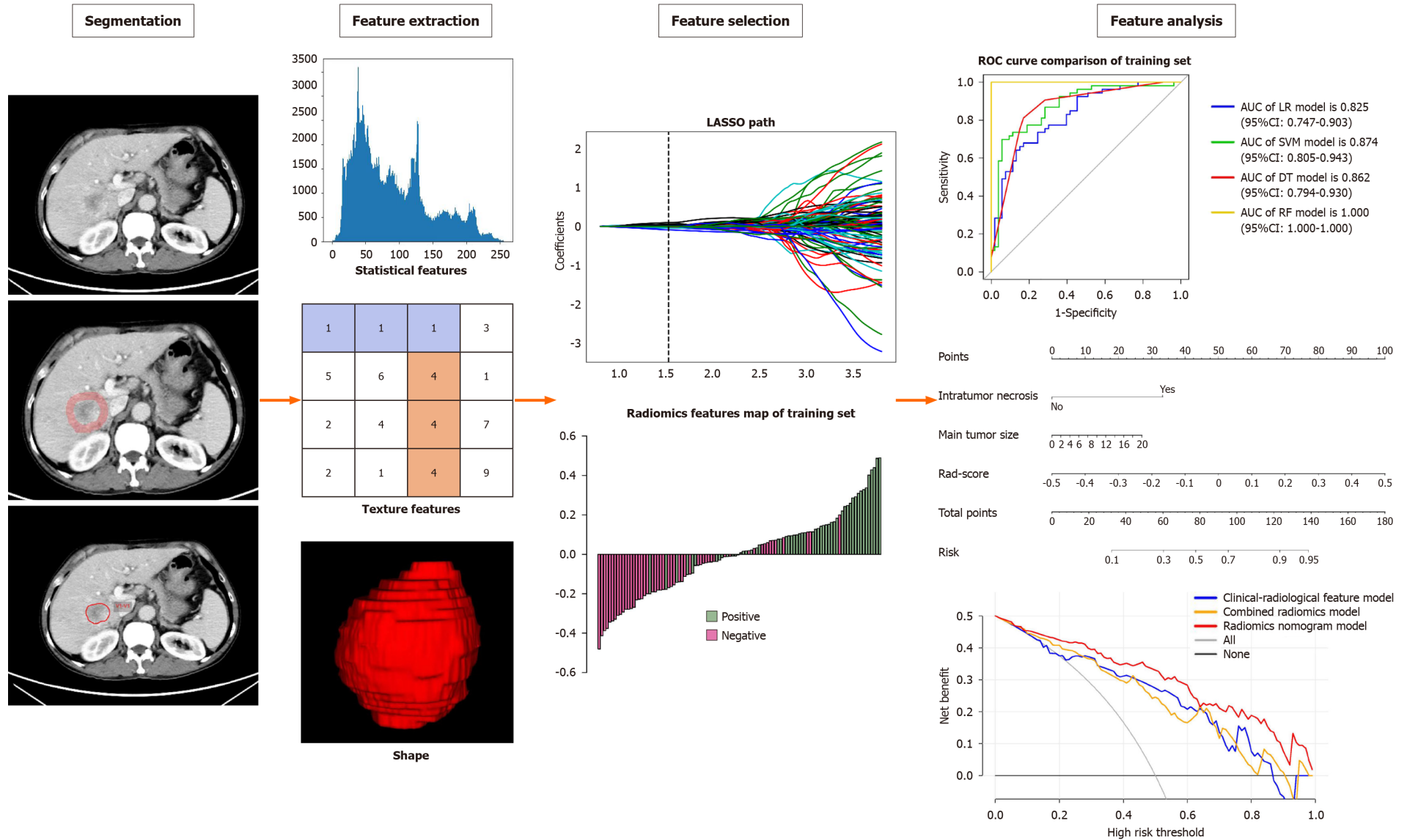


Figure 2 Flowchart of radiomics.

Development of radiomics feature and nomogram

We selected relevant features extracted from intratumoral, peritumoral, and combined intratumoral and peritumoral regions. Subsequently, a radiomics score (Rad-score) was computed for each patient by using LASSO logistic regression (LR) on the features, where the coefficients were utilized for weighting (refer to [Figure 3B](#)). Multiple machine learning algorithms, including LR, support vector machine (SVM), decision tree (DT), and random forest (RF), were employed to establish radiomics models for intratumoral, peritumoral, and combined regions. The model demonstrating the highest predictive performance among these algorithms was chosen to construct a radiomics nomogram in conjunction with the independent clinical-radiological feature.

Establishing the clinical-radiological feature model

The study recorded clinical and laboratory data, which included age, sex, history of hepatic virus infection [negative, history of hepatitis B virus (HBV), HCV, or HBV and HCV], history of cirrhosis (absent, present), alanine aminotransferase, aspartate aminotransferase, gamma-glutamyl transferase, and alpha-fetoprotein. The radiologists (reader 1 and reader 2) also reviewed radiological feature descriptors of each lesion, such as main tumor size, single lobe involvement, non-smooth tumor margin, intratumor necrosis, intratumor hemorrhage, AP hyperenhancement, washout, and well-defined capsule; occasional cases with discrepancies were referred to reader 3, were resolved by consensus. After multiple LR analysis, significant risk factors were used to build a clinical-radiological feature model.

Statistical analysis

Statistical analyses were carried out with the R software (version 4.2.1; <https://www.r-project.org/>). The Mann-Whitney *U* test was employed to assess the differences in clinical and radiological data among the three groups. Inter-group comparisons were performed using either the χ^2 test or one-way analysis of variance (ANOVA). Calibration curves were constructed based on 1000 iterations of bootstrap resampling, and the Hosmer-Lemeshow goodness-of-fit test was applied to evaluate the model calibration. To compare the estimated values of the area under the curve (AUC) for different prediction models, the non-parametric Delong test was utilized. All statistical tests were two-sided, and a significance level of $P < 0.05$ was considered statistically significant for the entire duration of the study.

RESULTS

Patient characteristics

The imaging of 190 preoperative patients with HCC was collected from two independent institutions in China. The training set included 106 patients from the center1 {male, 78%; median [interquartile range (IQR)] age 58.5 (51, 65.75)}, and the internal test set included 47 patients [male, 81%; median (IQR) age 56 (51.5, 67.5)]. The external test set came from the center2 [male, 86%; median (IQR) age 57 (50, 64)]. In the training set, 50% (53/106) of the patients were diagnosed with VETC+, 49% (23/47) were diagnosed with VETC+ in the internal set, and 49% (18/37) were diagnosed with VETC+ in the external set. There were no differences in clinical characteristics or radiological features between the training set and the two test sets ([Table 1](#)). The representative images of CECT and immunohistochemical staining for CD34 were shown in [Figure 4](#).

Clinical-radiological feature model construction

Details of the clinical data and the radiological features in the training set are provided in [Table 2](#). There was a statistically significant difference in the values of the 8 features selected by univariate analysis; these features were associated with VETC+ HCC and were considered as candidates for backward stepwise multivariate analysis. After multiple LR analysis, intratumor necrosis [$P < 0.001$, odds ratio (OR) = 7.947, 95% confidence interval (CI): 2.367-26.682] and main tumor size ($P < 0.001$, OR = 1.873, 95% CI: 0.629-5.581) were confirmed as independent predictors of VETC+ and were used to construct the clinical-radiological feature model ([Table 2](#)). Based on receiver operating characteristic (ROC) analysis, the AUCs for the clinical-radiological feature model was 0.833 (95% CI: 0.753-0.913), 0.781 (95% CI: 0.644-0.918), and 0.684 (95% CI: 0.498-0.862) in the training, internal test, and external test sets, respectively.

Feature selection and development of radiomics features

In total, 3376 radiomics features were extracted from two VOIs (1688 features for VOI-1, 1688 features for VOI-2). Among them, 1430 features from VOI-1 and 1328 features from VOI-2, both with an ICC > 0.8 , were retained for subsequent feature selection. The selection process involved applying the variance threshold, the SelectKBest and LASSO regression ([Figure 3A](#)).

After eliminating highly collinear features, we constructed the intratumoral (11 intratumoral features used), peritumoral (10 peritumoral features used), and combined (7 intratumoral and 6 peritumoral features used) radiomics models on the training set with multivariate LR ([Table 3](#)). Based on selected radiomics features, we built the intratumoral, peritumoral, and combined radiomics models.

Validation of radiomics feature models

The performance of the combined radiomics model in predicting VETC was evaluated using LR, SVM, DT, and RF ([Table 4](#) and [Figure 3](#)). Among these models, LR exhibited the best performance and was chosen as the classifier for all subsequent analyses in this article. The AUC for the intratumoral model was 0.772 (95% CI: 0.684-0.860) in the training set,

Table 1 Characteristic baseline of patients in sets

Variables	Total set (n = 190)	Training set (n = 106)	Internal test set (n = 47)	External test set (n = 37)	P value
VETC (%)					0.986
Positive	94 (49)	53 (50)	23 (49)	18 (49)	
Negative	96 (51)	53 (50)	24 (51)	19 (51)	
Age (median, IQR)	57 (51, 66)	58.5 (51, 65.75)	56 (51.5, 67.5)	57 (50, 64)	0.708
Sex (%)					0.555
Male	153 (81)	83 (78)	38 (81)	32 (86)	
Female	37 (19)	23 (22)	9 (19)	5 (14)	
Hepatitis (%)					0.799
HBV or/and HCV	171 (90)	96 (91)	41 (87)	34 (92)	
Negative	19 (10)	10 (9)	6 (13)	3 (8)	
Cirrhosis (%)					0.008
Present	158 (83)	85 (80)	36 (77)	37 (100)	
Absent	32 (17)	21 (20)	11 (23)	0 (0)	
ALT (median, IQR)	32 (19, 51.75)	28 (18, 49)	40 (22.5, 63)	33 (22, 45)	0.094
AST (median, IQR)	37 (25, 61.5)	36.5 (23.25, 1.75)	49 (28.5, 78)	30 (24, 46)	0.041
GGT (median, IQR)	59.25 (31, 131.25)	61.75 (30, 127)	76 (38.5, 143.5)	49 (27, 98)	0.157
AFP (median, IQR)	49.06 (5.54, 9.25)	62.74 (6.62, 9.25)	56.78 (5.87, 16.5)	34.74 (5.22, 798)	0.516
Main tumor size (median, IQR)	5.7 (3.2, 9.28)	6.05 (3.02, 9.3)	6.9 (3.45, 11.15)	4.11 (3.2, 6.5)	0.098
Multiplicity (%)					0.037
≥ 2	46 (24)	29 (27)	14 (30)	3 (8)	
1	144 (76)	77 (73)	33 (70)	34 (92)	
Single lobe involvement (%)					0.064
Present	141 (74)	74 (70)	34 (72)	33 (89)	
Absent	49 (26)	32 (30)	13 (28)	4 (11)	
Intratumor hemorrhage (%)					0.179
Present	12 (6)	9 (8)	3 (6)	0 (0)	
Absent	178 (94)	97 (92)	44 (94)	37 (100)	
Intratumor necrosis (%)					0.131
Present	95 (50)	57 (54)	25 (53)	13 (35)	
Absent	95 (50)	49 (46)	22 (47)	24 (65)	
Arterial phase hyper enhancement (%)					0.701
Present	179 (94)	101 (95)	44 (94)	34 (92)	
Absent	11 (6)	5 (5)	3 (6)	3 (8)	
Well defined capsule (%)					0.143
Present	140 (74)	75 (71)	33 (70)	32 (86)	
Absent	50 (26)	31 (29)	14 (30)	5 (14)	
Washout (%)					0.249
Present	187 (98)	105 (99)	45 (96)	37 (100)	
Absent	3 (2)	1 (1)	2 (4)	0 (0)	

Non-smooth tumor margin (%)					0.435
Present	116 (61)	69 (65)	26 (55)	21 (57)	
Absent	74 (39)	37 (35)	21 (45)	16 (43)	

VETC: Vessels encapsulating tumor cluster; IQR: Interquartile range; HBV: Hepatitis B virus; HCV: Hepatitis C virus; ALT: Alanine aminotransferase; AST: Aspartate aminotransferase; GGT: Gamma-glutamyl transferase; AFP: Alpha-fetoprotein.

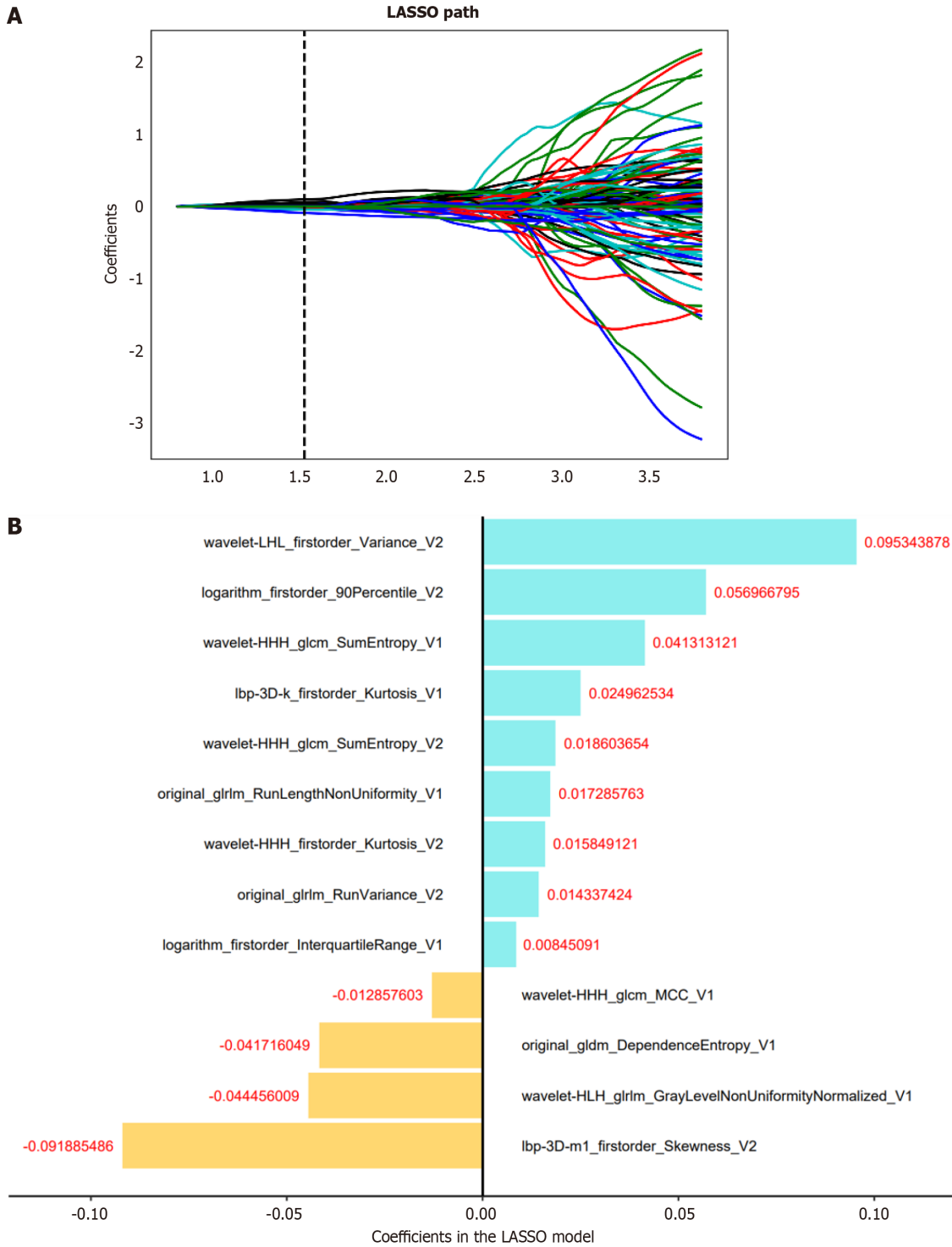


Figure 3 Radiomics feature selection. A: The least absolute shrinkage and selection operator of the parameterized method was used to select the image omics features by logistic regression; select the optimal alpha of 0.0297 with log(alpha) of -1.527; B: The coefficients of the radiomics features were used for weighting. LASSO: Least absolute shrinkage and selection operator.

Table 2 Univariable and Multivariable logistic regression for upstaging in the training set

Variables	VETC- (<i>n</i> = 53)	VETC+ (<i>n</i> = 53)	Univariate analysis		Multivariate analysis	
			OR	<i>P</i> value	OR	<i>P</i> value
Age, median (IQR)	63 (50, 67)	55 (51, 62)	0.997	0.096		
Sex (%)			1.344	0.637		
Male	40 (75)	43 (81)				
Female	13 (25)	10 (19)				
Hepatitis (%)			1.133	0.74		
HBV or/and HCV	47 (89)	49 (92)				
Negative	6 (11)	4 (8)				
Cirrhosis (%)			0.669	0.626		
Present	44 (83)	41 (77)				
Absent	9 (17)	12 (23)				
ALT, median (IQR)	23 (15, 38)	36 (20, 52)	1.010	0.011	1.001	0.738
AST, median (IQR)	29 (21, 50)	40 (28, 68)	0.989	0.022	0.991	0.450
GGT, median (IQR)	39 (27, 87)	100 (40, 185)	1.000	0.001	1.000	0.209
AFP, median (IQR)	62.23 (5.48, 446.4)	78.51 (8.05, 8213)	0.999	0.076		
Main tumor size, median (IQR)	4.1 (2.4, 6.5)	8.9 (5.6, 10.8)	2.815	< 0.001	1.873	< 0.001
Multiplicity (%)			0.799	0.009	0.907	0.660
≥ 2	8 (15)	21 (40)				
1	45 (85)	32 (60)				
Single lobe involvement (%)			0.620	< 0.001	0.952	0.617
Present	46 (87)	28 (53)				
Absent	7 (13)	25 (47)				
Intratumor hemorrhage (%)			0.609	1		
Present	4 (8)	5 (9)				
Absent	49 (92)	48 (91)				
Intratumor necrosis (%)			0.850	< 0.001	7.947	< 0.001
Present	13 (25)	44 (83)				
Absent	40 (75)	9 (17)				
Arterial phase hyperenhancement (%)			1.112	0.363		
Present	49 (92)	52 (98)				
Absent	4 (8)	1 (2)				
Well defined capsule (%)			1.018	1		
Present	38 (72)	37 (70)				
Absent	15 (28)	16 (30)				
Washout (%)			1.815	1		
Present	52 (98)	53 (100)				
Absent	1 (2)	0 (0)				
Non-smooth tumor margin (%)			1.717	0.014	1.109	0.881
Present	28 (53)	41 (77)				
Absent	25 (47)	12 (23)				

VETC: Vessels encapsulating tumor cluster; IQR: Interquartile range; HBV: Hepatitis B virus; HCV: Hepatitis C virus; ALT: Alanine aminotransferase; AST: Aspartate aminotransferase; GGT: Gamma-glutamyl transferase; AFP: Alpha-fetoprotein.

Table 3 Selected radiomics features in intratumoral, peritumoral, and combined radiomics models on the training set

Intratumoral radiomics model	Peritumoral radiomics model	Combined radiomics model
Original_GLDM_DependenceEntropy	Original_shape_Sphericity	Original_GLDM_DependenceEntropy ¹
Lbp-3D-k_GLRLM_ShortRunHighGrayLevelEmphasis	Lbp-2D_firstorder_InterquartileRange	Original_GLRLM_RunLengthNonUniformity ¹
Lbp-3D-k_GLDM_SmallDependenceEmphasis	Lbp-3D-k_firstorder_Minimum	Wavelet-HHH_GLCM_SumEntropy ¹
Original_GLRLM_RunLengthNonUniformity	Wavelet-HHH_GLCM_SumEntropy	Wavelet-HHH_GLCM_SumEntropy ²
Wavelet-HHH_GLCM_SumEntropy	Original_GLRLM_RunVariance	Original_GLRLM_RunVariance ²
Lbp-3D-k_firstorder_Kurtosis	Wavelet-LHL_firstorder_Variance	Logarithm_firstorder_InterquartileRange ¹
Wavelet-HLH_GLRLM_GrayLevelNonUniformityNormalized	Lbp-3D-m1_firstorder_Skewness	Wavelet-LHL_firstorder_Variance ²
Squareroot_firstorder_Minimum	Logarithm_firstorder_10Percentile	Wavelet-HHH_GLCM_MCC ¹
Wavelet-LLH_GLCM_Imc2	Squareroot_firstorder_10Percentile	Lbp-3D-k_firstorder_Kurtosis ¹
Wavelet-LHL_GLCM_MaximumProbability	Wavelet-HLL_firstorder_Kurtosis	Wavelet-HHH_firstorder_Kurtosis ²
Wavelet-HLH_GLCM_MaximumProbability		Lbp-3D-m1_firstorder_Skewness ²
		Wavelet-HLH_GLRLM_GrayLevelNonUniformityNormalized_V1 ¹
		Logarithm_firstorder_90Percentile ²

¹Intratumoral radiomics.

²Peritumoral radiomics.

GLRLM: Gray level run length matrix; GLCM: Gray level co-occurrence matrix; GLDM: Gray level dependence matrix; Lbp-2D: Local binary pattern in 2D; Lbp-3D: Local binary pattern in 3D.

0.768 (95% CI: 0.628-0.908) in the internal test set, and 0.673 (95% CI: 0.495-0.851) in the external test set. For the peritumoral model, the AUC values were 0.823 (95% CI: 0.745-0.901) in the training set, 0.757 (95% CI: 0.615-0.899) in the internal test set, and 0.605 (95% CI: 0.418-0.792) in the external test set. The combined radiomics model demonstrated the highest predictive performance across the training set and both test sets, with AUC values of 0.825 (95% CI: 0.747-0.903) in the training set, 0.788 (95% CI: 0.649-0.927) in the internal test set, and 0.680 (95% CI: 0.498-0.862) in the external test set (Table 5 and Figure 5).

Development of a radiomics nomogram and evaluation of model performance

To develop a clinically applicable approach that could predict the probability of VETC+ HCC, the clinical-radiological and radiomics features were incorporated into the radiomics nomogram (Figure 6A). The Rad-score, calculated by applying LR to the combined radiomics features weighted by their coefficients, served as an indicator for each patient. The calibration curves of the radiomics nomogram demonstrated a satisfactory fit in the training, internal test and external test sets (Figure 6B-D), as evidenced by the Hosmer-Lemeshow test *P*-values of 0.8633, 0.7965, and 0.3205 respectively, which indicate the goodness-of-fit of the model. As shown in the nomogram (Figure 6A), by assigning each feature a value based on a point scale ranging from 0 to 100, one can obtain a total score by adding the scores for each feature. The risk of VETC+ HCC can be predicted by projecting the score to the bottom risk axis. The sensitivity, specificity, accuracy, and AUC of the clinical-radiological feature, combined radiomics, and radiomics nomogram models are shown in Table 6. The radiomics nomogram exhibited superior predictive performance, with an AUC of 0.859 (95% CI: 0.787-0.931) on the training set, 0.848 (95% CI: 0.726-0.970) on the internal test set, and 0.757 (95% CI: 0.592-0.922) on the external test set, and achieved better discriminatory performance than the clinical-radiological feature and the combined radiomics models (Figure 7A-C). The Delong test revealed statistically significant differences in AUCs among the clinical-radiological feature, the combined radiomics and the radiomics nomogram models on the internal test set (*P* = 0.004 and *P* < 0.001, respectively). The utility of the three predictive models was assessed using DCA, which calculated the net benefit at various probability thresholds (Figure 7D-F). The DCA results indicated that the radiomics nomogram model provided greater overall net benefit than either the radiological feature or the combined radiomics models, affirming the reliability of the nomogram as a clinical tool for predicting the risk of VETC+ HCC.

Table 4 Performance of logistic regression, support vector machine, decision tree, and random forest in the combined radiomics for predicting vessels encapsulating tumor clusters

Set	ML model	AUC (95%CI)	Accuracy	Sensitivity	Specificity	PPV	NPV
Training							
	LR	0.825 (0.747-0.903)	0.726	0.736	0.717	0.722	0.731
	SVM	0.874 (0.805-0.943)	0.764	0.792	0.736	0.745	0.765
	DT	0.862 (0.794-0.930)	0.820	0.811	0.830	0.827	0.815
	RF	1 (1.000-1.000)	1	1	1	1	1
Internal test							
	LR	0.788 (0.649-0.927)	0.745	0.783	0.708	0.720	0.773
	SVM	0.766 (0.629-0.903)	0.681	0.739	0.625	0.654	0.714
	DT	0.698 (0.556-0.840)	0.659	0.696	0.625	0.640	0.682
	RF	0.723 (0.577-0.869)	0.702	0.739	0.667	0.667	0.696
External test							
	LR	0.680 (0.498-0.862)	0.676	0.500	0.842	0.750	0.640
	SVM	0.632 (0.438-0.826)	0.676	0.500	0.842	0.75	0.640
	DT	0.667 (0.482-0.852)	0.676	0.500	0.842	0.750	0.640
	RF	0.614 (0.428-0.800)	0.568	0.444	0.684	0.571	0.565

LR: Logistic regression; SVM: Support vector machine; DT: Decision tree; RF: Random forest; CI: Confidence interval; AUC: Area under the curve; PPV: Positive predictive value; NPV: Negative predictive value.

Table 5 Performance evaluation of the logistic regression models on the training set and the two test sets

Set	Model	AUC (95%CI)	Accuracy	Sensitivity	Specificity	PPV	NPV
Training							
	Intratumoral radiomics	0.772 (0.684-0.860)	0.689	0.736	0.642	0.673	0.708
	Peritumoral radiomics	0.823 (0.745-0.901)	0.745	0.774	0.717	0.732	0.760
	Combined radiomics	0.825 (0.747-0.903)	0.726	0.736	0.717	0.722	0.731
Internal test							
	Intratumoral radiomics	0.768 (0.628-0.908)	0.638	0.696	0.583	0.615	0.667
	Peritumoral radiomics	0.757 (0.615-0.899)	0.702	0.783	0.625	0.750	0.667
	Combined radiomics	0.788 (0.649-0.927)	0.745	0.783	0.708	0.720	0.773
External test							
	Intratumoral radiomics	0.673 (0.495-0.851)	0.568	0.556	0.579	0.556	0.579
	Peritumoral radiomics	0.605 (0.418-0.792)	0.568	0.389	0.737	0.560	0.583
	Combined radiomics	0.680 (0.498-0.862)	0.676	0.500	0.842	0.750	0.640

CI: Confidence interval; AUC: Area under the curve; PPV: Positive predictive value; NPV: Negative predictive value.

DISCUSSION

The VETC pattern in HCC has been identified as a predictor of micro-metastasis, aggressive behavior, and unfavorable prognosis[13,26]. There is a lack of development and validation for CT radiomics model to preoperatively predict the VETC subtype of HCC, and the biologic underpinnings of the radiomics method deserve investigation. In our study, we established and validated a noninvasive CECT radiomics nomogram composed of radiomics features, and the clinical-radiological feature of intratumor necrosis, and main tumor size predict VETC+. Our results showed that the combined radiomics model showed no additional value over the clinical-radiological feature model, but that the nomogram showed

Table 6 Diagnostic performance of the clinical-radiological feature, combined radiomics, and radiomics nomogram models

Set	Model	AUC (95%CI)	Accuracy	Sensitivity	Specificity	PPV	NPV
Training							
	Clinical-radiological feature	0.833 (0.753-0.913)	0.792	0.830	0.754	0.737	0.776
	Combined radiomics	0.825 (0.747-0.903)	0.726	0.736	0.717	0.722	0.731
	Radiomics nomogram	0.859 (0.787-0.931)	0.792	0.830	0.754	0.772	0.816
Internal test							
	Clinical-radiological feature	0.781 (0.644-0.918)	0.744	0.782	0.708	0.720	0.773
	Combined radiomics	0.788 (0.649-0.927)	0.745	0.783	0.709	0.720	0.773
	Radiomics nomogram	0.848 (0.726-0.970)	0.787	0.826	0.750	0.760	0.818
External test							
	Clinical-radiological feature	0.684 (0.498-0.862)	0.676	0.500	0.842	0.750	0.64
	Combined radiomics	0.680 (0.502-0.866)	0.676	0.500	0.842	0.750	0.640
	Radiomics nomogram	0.757 (0.592-0.922)	0.729	0.611	0.842	0.750	0.783

CI: Confidence interval; AUC: Area under the curve; PPV: Positive predictive value; NPV: Negative predictive value.

good discrimination performance (AUC: 0.859) on the training set and the two test sets for prediction of VETC+ compared with the combined radiomics model or the clinical-radiological feature model.

Feng *et al*[27] had reported that the presence of VETC demonstrated a significant correlation with various clinical characteristics, including tumor size exceeding 5 cm and the occurrence of tumor necrosis. In our study, maximum tumor diameter and tumor necrosis were also independent predictors for VETC subtype. This agrees with the findings reported by them in the clinical-radiological feature model which achieved areas under the ROC curve of 0.833, 0.781, and 0.684 on the training set, the internal test set and the external test set, respectively. Angiogenesis activation is a mark of aggressive VETC HCC. Increased diffusion distances from the existing vascularity supply as the tumor expands and increased cellularity due to proliferative tumor cells result in hypoxia and necrosis. Hypoxia and neoangiogenesis result in obvious necrosis in fast-growing HCC[28,29]. Neovascularity mainly occurs on the periphery of the tumor, and rapidly reduces central perfusion, leading to central necrosis.

Radiomics has been known as an important digital biopsy method to predict several biological features of tumors[12]. In this study, we constructed a machine learning-based CECT radiomics model, performed canonical screening of features and multiple validations, and confirmed robustness on various data resources. The suboptimal performance on the external test set may be ascribed to differences in the CT scan protocol and to heterogeneity of the data set, which came from two different institutions. However, the radiomics model showed remarkable performance in predicting the VETC subtype, and the results were reproducible, demonstrating that the approach may be applied to other patient samples. VETC is a heterogeneous pattern of angiogenesis involved in HCC biological behavior[12]. This may account for why the radiomics model had a favorable predictive ability in predicting VETC. In this study, the intratumoral or peritumoral radiomics model achieved identified good performance in predicting VETC. As shown in our study, the peritumoral radiomics model was superior to the intratumoral model, which was consistent with previous reports[20,30]. This result might suggest that VETC is more likely to be found in the peritumoral region. Moreover, the combined intratumoral and peritumoral radiomics model exhibited better predictive performance than the intratumoral model in preoperative prediction of VETC in HCC. Furthermore, we combined the clinical-radiological feature and the radiomics models to create the radiomics nomogram model and validate its predictive power. Our study showed that the radiomics nomogram model had a higher predictive value than the single clinical-radiological feature model or the radiomics model with, AUC of 0.859, 0.848, and 0.757 on the training set, the internal test set and the external test set, respectively. Our result goes further by indicating a radiomics link between CT imaging and VETC subtype, which may facilitate the implementation of morphomolecular subtyping of HCC into clinical practice and application.

The radiomics model could reflect the heterogeneity of HCC[31]. First-order features mainly depend on the statistics of the intensity information. Texture analysis was recently found to provide a quantitative, objective assessment of tumor heterogeneity by analyzing the distribution and relationship of pixel or voxel grey levels and could reflect information on the lesion microenvironment[32]. In our study, of the eleven features in the intratumoral radiomics model, two were first-order features and nine were texture features. Of the ten features in the peritumoral radiomics model, seven were first-order features, one was a shape feature, and only two were texture features. The radiomics model had more texture features, especially the intratumoral radiomics model. The results demonstrated that VETC+ HCC have more diverse vascular patterns, including VETC, sinusoidal capillarization and other neovascularization patterns, which could lead to additional heterogeneity in texture compared with VETC- HCC.

Our study had several limitations. First, the radiomics model was constructed based on retrospective data with patients who underwent surgical or biopsy treatments at multiple institutions, which may have resulted in selection bias.

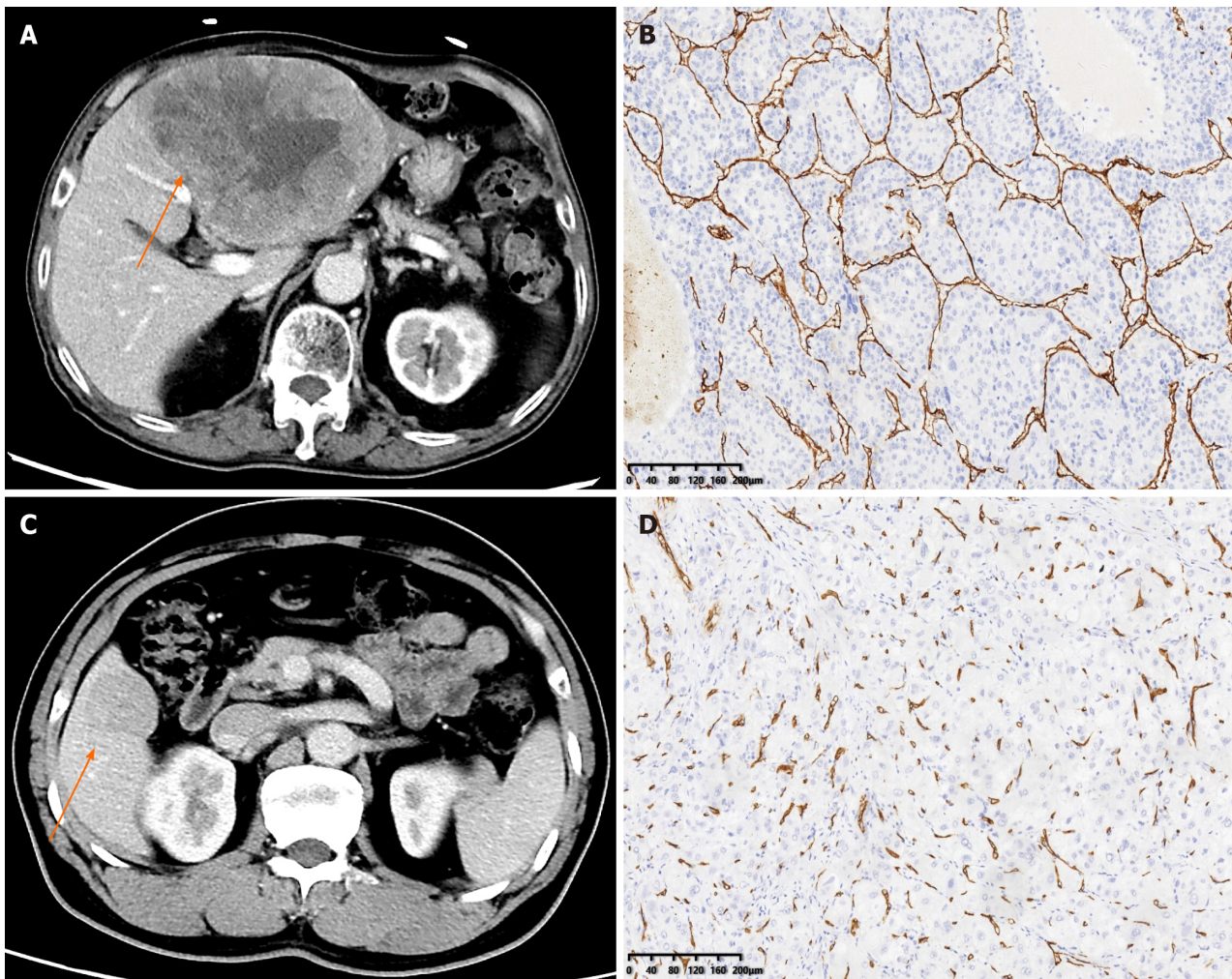


Figure 4 Contrast enhanced computed tomography and immunohistochemical staining for cluster of differentiation 34. A: Vessels encapsulating tumor cluster (VETC) + hepatocellular carcinoma (HCC) in a 71-year-old man, a mass (the arrow) can be seen in the lateral left lobe of liver; B: Immunohistochemical image for cluster of differentiation 34 (CD34) presented vessels that encapsulated tumor clusters and formed cobweb-like networks (original magnification, $\times 100$); C: VETC-HCC in a 52-year-old man, a mass (the arrow) can be seen in the anterior right lobe of the liver; D: Immunohistochemical image for CD34 presented vessels with discrete lumens (original magnification, $\times 100$).

Second, we defined “VETC $\geq 5\%$ ” as the VETC group [12,33] with reference to previous reports. However, the optimal cut-off value of VETC is not yet standardized. Future studies could be conducted to develop and verify the optimal cut-off value for HCC. Third, the sample size of our study was relatively small, especially the external validation group, and larger sample sizes are needed for radiomics analysis in future studies. Finally, the radiomics marker is limited by its complexity and lack of algorithmic standardization. In future studies, the development of a deep learning-based predictive model will be constructed and validated. Therefore, a further prospective study avoiding the above limitations is needed to validate those results.

CONCLUSION

In conclusion, the CECT radiomics model could noninvasively predict the VETC subtype in patients with HCC. The radiomics nomogram constructed from clinical-radiological features and combined radiomics features demonstrated good performance in preoperatively predicting VETC, and their combination showed superior predictive performance compared with the single model. Thus, this combination may be useful for the preoperative identification of VETC subtype in HCC, which could help select HCC patients with poor prognosis, early recurrence, and Sorafenib benefit. Therefore, it could provide valuable information for assisting clinicians in pretreatment decision-making.

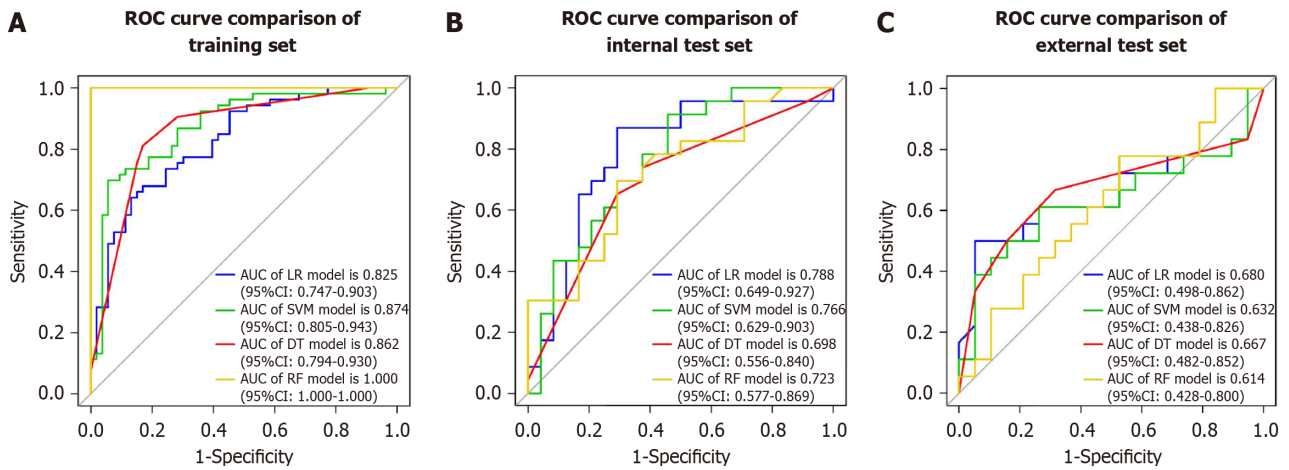


Figure 5 Receiver operating characteristic of the combined radiomics models. A: Receiver operating characteristic (ROC) of combined radiomics model using four machine learning algorithms on the training set; B: ROC of combined radiomics model using four machine learning algorithms on the internal test set; C: ROC of combined radiomics model using four machine learning algorithms on the external test set. ROC: Receiver operating characteristic; LR: Logistic regression; SVM: Support vector machine; DT: Decision tree; RF: Random forest; CI: Confidence interval; AUC: Area under the curve.

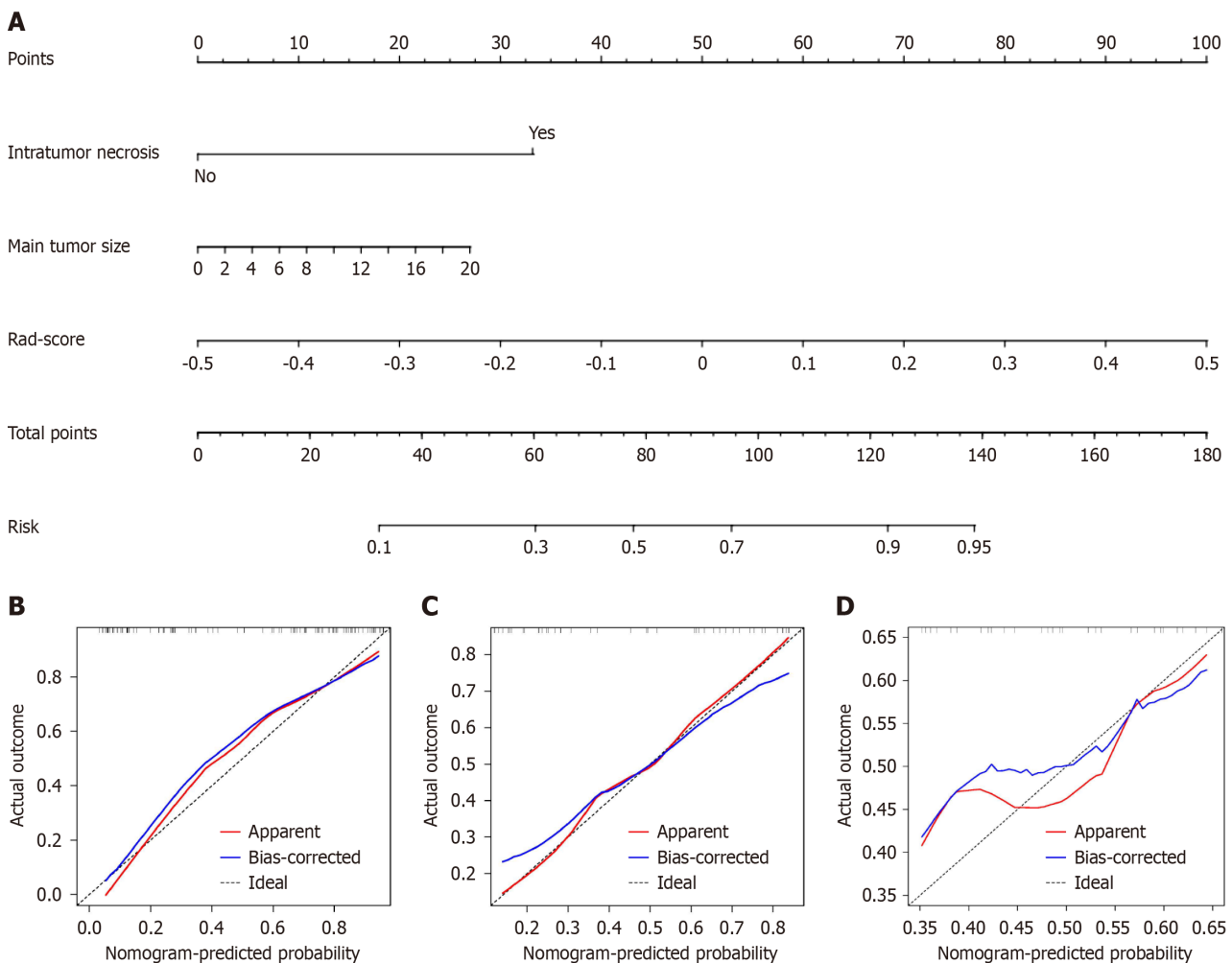


Figure 6 The radiomics nomogram and calibration curves for the radiomics nomogram. A: The radiomics nomogram combining intratumor necrosis, main tumor size, and radiomics score, was developed on the training set; B: Calibration curves for the radiomics nomogram on the training set; C: Calibration curves for the radiomics nomogram on the internal test set; D: Calibration curves for the radiomics nomogram on the external test set.

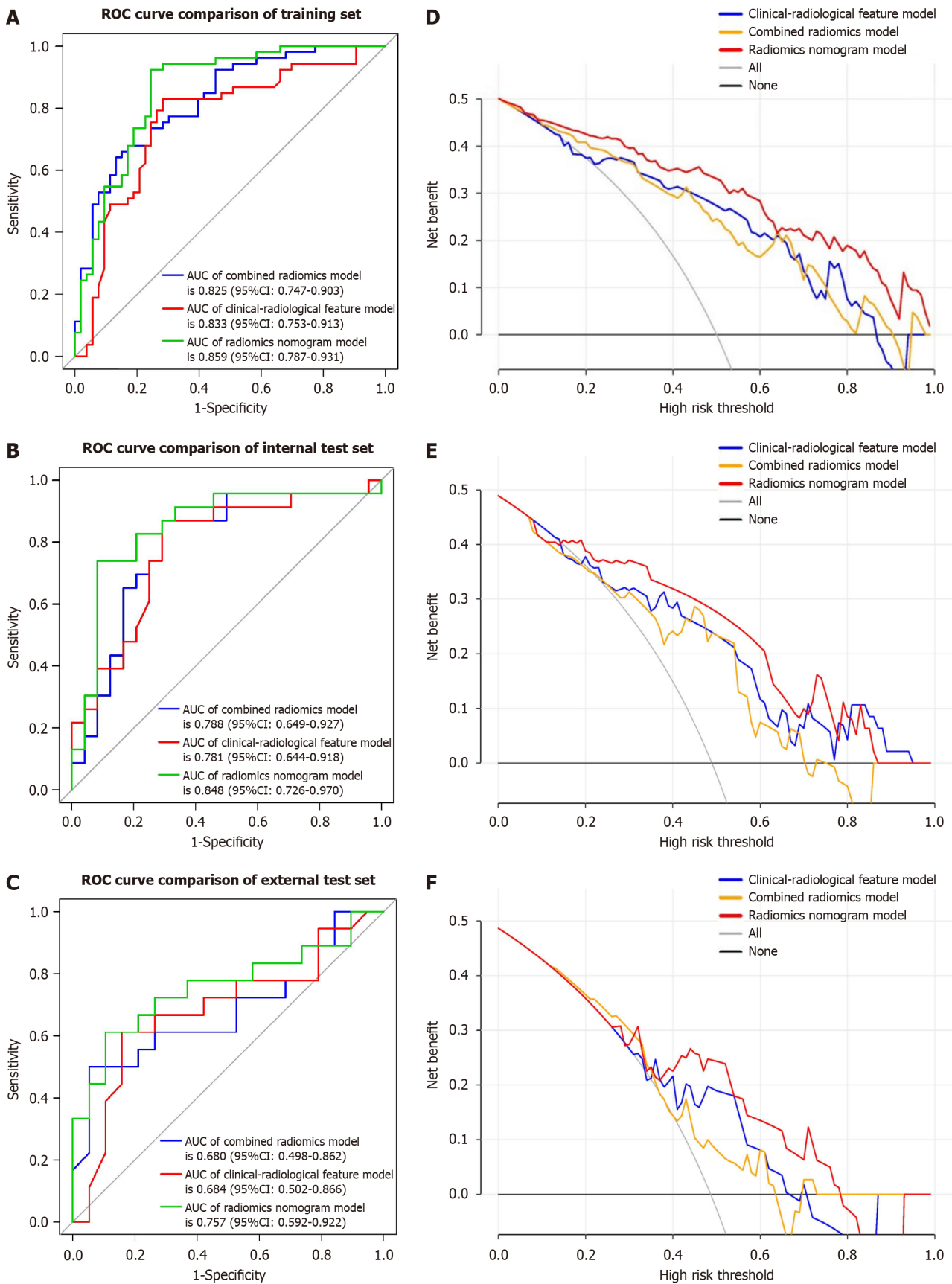


Figure 7 Receiver operating characteristic and decision curve analysis for three models. A: Receiver operating characteristic (ROC) of clinical-radiological features on the training set; B: ROC of clinical-radiological features on the internal test set; C: ROC of clinical-radiological features on the external test set; D: Decision curve analysis on the training set; E: Decision curve analysis on the internal test set; F: Decision curve anal. ROC: Receiver operating characteristic; CI: Confidence interval; AUC: Area under the curve.

ARTICLE HIGHLIGHTS

Research background

Vessels encapsulating tumor clusters (VETC) is an independent risk factor for poor prognosis in hepatocellular carcinoma (HCC) and patients with VETC+ HCC show shorter overall survival and disease-free survival and are more prone to progression and metastasis relative to patients with VETC- HCC. So far, VETC is currently determined only on histologic examination after surgical resection.

Research motivation

Preoperative diagnosis of VETC status in HCC is of great significance for predicting the prognosis of HCC patients and determining treatment strategies.

Research objectives

This study aimed to develop and validate a preoperative nomogram based on contrast-enhanced computed tomography (CECT) scanning combined with radiomics and clinical-radiological features to provide a preoperative reference for accurate prediction of VETC status in patients with HCC.

Research methods

This was a retrospective, diagnostic study conducted from January 2017 to March 2023, at two centers. The study included 190 (training set: 106; internal test set: 47; external test set: 37) HCC patients who underwent CECT. Variance threshold, SelectKBest, the least absolute shrinkage and selection operator algorithm and multivariable logistic regression analysis were used to select the useful features and transform them into models. Receiver operating characteristic analysis was employed to compare the identified performance of models in predicting the VETC status of HCC on both training and test sets.

Research results

Among 190 individuals used for radiomics modeling, with the majority being male (81%) and a median age of 57 years (interquartile range: 51-66), 94 (49%) were confirmed to have the VETC subtype. The nomogram model included clinical-radiological features and 13 radiomics features and showed good performance for predicting the VETC subtype, with area under the curves of 0.859, 0.848, and 0.757 in the training set, internal test set, and external test set, respectively. The radiomics nomogram outperformed any clinical-radiological feature and the combined radiomics models in terms of clinical predictive abilities, according to a decision curve analysis.

Research conclusions

The findings of this research indicate that a nomogram, developed using clinical-radiological features and combined radiomics features, holds the capability to accurately forecast the VETC status of HCC.

Research perspectives

Our findings may be useful for preoperative identification of VETC subtype in HCC, which could help select HCC patients with poor prognosis, early recurrence, and sorafenib benefit.

FOOTNOTES

Co-first authors: Chao Zhang and Hai Zhong.

Author contributions: Zhang C, Zhong H, and Pang GD designed the research study, analyzed the data, and wrote the manuscript; Zhao F and Ma ZY performed the research; Dai ZJ contributed new reagents and analytic tools; and all authors have read and approve the final manuscript.

Institutional review board statement: The study was reviewed and approved by the Second Hospital of Shandong University Institutional Review Board, IRB No. KYLL-2023LW044.

Informed consent statement: The requirement for informed consent was waived because of the retrospective data sets.

Conflict-of-interest statement: All the authors report no relevant conflicts of interest for this article.

Data sharing statement: Technical appendix, statistical code and dataset available from corresponding author at pgd226@aliyun.com.

Open-Access: This article is an open-access article that was selected by an in-house editor and fully peer-reviewed by external reviewers. It is distributed in accordance with the Creative Commons Attribution NonCommercial (CC BY-NC 4.0) license, which permits others to distribute, remix, adapt, build upon this work non-commercially, and license their derivative works on different terms, provided the original work is properly cited and the use is non-commercial. See: <https://creativecommons.org/licenses/by-nc/4.0/>

Country/Territory of origin: China

ORCID number: Guo-Dong Pang 0000-0002-2622-1616.

S-Editor: Wang JJ

L-Editor: A

P-Editor: Zheng XM

REFERENCES

- Huang X, Long L, Wei J, Li Y, Xia Y, Zuo P, Chai X. Radiomics for diagnosis of dual-phenotype hepatocellular carcinoma using Gd-EOB-DTPA-enhanced MRI and patient prognosis. *J Cancer Res Clin Oncol* 2019; **145**: 2995-3003 [PMID: 31664520 DOI: 10.1007/s00432-019-03062-3]
- Shao CC, Zhao F, Yu YF, Zhu LL, Pang GD. Value of perfusion parameters and histogram analysis of triphasic computed tomography in pre-operative prediction of histological grade of hepatocellular carcinoma. *Chin Med J (Engl)* 2021; **134**: 1181-1190 [PMID: 34018996 DOI: 10.1097/CM9.0000000000001446]
- Bray F, Ferlay J, Soerjomataram I, Siegel RL, Torre LA, Jemal A. Global cancer statistics 2018: GLOBOCAN estimates of incidence and mortality worldwide for 36 cancers in 185 countries. *CA Cancer J Clin* 2018; **68**: 394-424 [PMID: 30207593 DOI: 10.3322/caac.21492]
- Tabrizian P, Jibara G, Shrager B, Schwartz M, Roayaie S. Recurrence of hepatocellular cancer after resection: patterns, treatments, and prognosis. *Ann Surg* 2015; **261**: 947-955 [PMID: 25010665 DOI: 10.1097/SLA.0000000000000710]
- Ma X, Wei J, Gu D, Zhu Y, Feng B, Liang M, Wang S, Zhao X, Tian J. Preoperative radiomics nomogram for microvascular invasion prediction in hepatocellular carcinoma using contrast-enhanced CT. *Eur Radiol* 2019; **29**: 3595-3605 [PMID: 30770969 DOI: 10.1007/s00330-018-5985-y]
- Fang JH, Zhou HC, Zhang C, Shang LR, Zhang L, Xu J, Zheng L, Yuan Y, Guo RP, Jia WH, Yun JP, Chen MS, Zhang Y, Zhuang SM. A novel vascular pattern promotes metastasis of hepatocellular carcinoma in an epithelial-mesenchymal transition-independent manner. *Hepatology* 2015; **62**: 452-465 [PMID: 25711742 DOI: 10.1002/hep.27760]
- Morse MA, Sun W, Kim R, He AR, Abada PB, Mynderse M, Finn RS. The Role of Angiogenesis in Hepatocellular Carcinoma. *Clin Cancer Res* 2019; **25**: 912-920 [PMID: 30274981 DOI: 10.1158/1078-0432.CCR-18-1254]
- Zhu AX, Duda DG, Sahani DV, Jain RK. HCC and angiogenesis: possible targets and future directions. *Nat Rev Clin Oncol* 2011; **8**: 292-301 [PMID: 21386818 DOI: 10.1038/nrclinonc.2011.30]
- Giannelli G, Koudelkova P, Dituri F, Mikulits W. Role of epithelial to mesenchymal transition in hepatocellular carcinoma. *J Hepatol* 2016; **65**: 798-808 [PMID: 27212245 DOI: 10.1016/j.jhep.2016.05.007]
- Zeng HX, Li Z, Chen JG, Fang JH, Zhuang SM. [Vessels Encapsulating Tumor Clusters (VETC): a New Mechanism of Tumor Metastasis and A New Target for Precision Medicine]. *Chinese J Cell Biol* 2022
- Chen ZY, Guo ZX, Lu LH, Mei J, Lin WP, Li SH, Wei W, Guo RP. The predictive value of vessels encapsulating tumor clusters in treatment optimization for recurrent early-stage hepatocellular carcinoma. *Cancer Med* 2021; **10**: 5466-5474 [PMID: 34212527 DOI: 10.1002/cam4.4102]
- Renne SL, Woo HY, Allegra S, Rudini N, Yano H, Donadon M, Viganò L, Akiba J, Lee HS, Rhee H, Park YN, Roncalli M, Di Tommaso L. Vessels Encapsulating Tumor Clusters (VETC) Is a Powerful Predictor of Aggressive Hepatocellular Carcinoma. *Hepatology* 2020; **71**: 183-195 [PMID: 31206715 DOI: 10.1002/hep.30814]
- Fang JH, Xu L, Shang LR, Pan CZ, Ding J, Tang YQ, Liu H, Liu CX, Zheng JL, Zhang YJ, Zhou ZG, Xu J, Zheng L, Chen MS, Zhuang SM. Vessels That Encapsulate Tumor Clusters (VETC) Pattern Is a Predictor of Sorafenib Benefit in Patients with Hepatocellular Carcinoma. *Hepatology* 2019; **70**: 824-839 [PMID: 30506570 DOI: 10.1002/hep.30366]
- Zhu YY, Chen F. [A novel tumor vascular metastasis pathway and its imaging research progress in hepatocellular carcinoma: vessels encapsulating tumor clusters]. *Chinese J Radiol* 2023; **57**: 101-105 [DOI: 10.3760/cma.j.cn112149-20220113-00039]
- Gillies RJ, Kinahan PE, Hricak H. Radiomics: Images Are More than Pictures, They Are Data. *Radiology* 2016; **278**: 563-577 [PMID: 26579733 DOI: 10.1148/radiol.2015151169]
- Yang L, Yang J, Zhou X, Huang L, Zhao W, Wang T, Zhuang J, Tian J. Development of a radiomics nomogram based on the 2D and 3D CT features to predict the survival of non-small cell lung cancer patients. *Eur Radiol* 2019; **29**: 2196-2206 [PMID: 30523451 DOI: 10.1007/s00330-018-5770-y]
- Wu M, Tan H, Gao F, Hai J, Ning P, Chen J, Zhu S, Wang M, Dou S, Shi D. Predicting the grade of hepatocellular carcinoma based on non-contrast-enhanced MRI radiomics signature. *Eur Radiol* 2019; **29**: 2802-2811 [PMID: 30406313 DOI: 10.1007/s00330-018-5787-2]
- Wu J, Liu A, Cui J, Chen A, Song Q, Xie L. Radiomics-based classification of hepatocellular carcinoma and hepatic haemangioma on precontrast magnetic resonance images. *BMC Med Imaging* 2019; **19**: 23 [PMID: 30866850 DOI: 10.1186/s12880-019-0321-9]
- Shan QY, Hu HT, Feng ST, Peng ZP, Chen SL, Zhou Q, Li X, Xie XY, Lu MD, Wang W, Kuang M. CT-based peritumoral radiomics signatures to predict early recurrence in hepatocellular carcinoma after curative tumor resection or ablation. *Cancer Imaging* 2019; **19**: 11 [PMID: 30813956 DOI: 10.1186/s40644-019-0197-5]
- Yu Y, Fan Y, Wang X, Zhu M, Hu M, Shi C, Hu C. Gd-EOB-DTPA-enhanced MRI radiomics to predict vessels encapsulating tumor clusters (VETC) and patient prognosis in hepatocellular carcinoma. *Eur Radiol* 2022; **32**: 959-970 [PMID: 34480625 DOI: 10.1007/s00330-021-08250-9]
- Dong X, Yang J, Zhang B, Li Y, Wang G, Chen J, Wei Y, Zhang H, Chen Q, Jin S, Wang L, He H, Gan M, Ji W. Deep Learning Radiomics Model of Dynamic Contrast-Enhanced MRI for Evaluating Vessels Encapsulating Tumor Clusters and Prognosis in Hepatocellular Carcinoma. *JMRI* 2023; **59**: 108-119 [DOI: 10.1002/jmri.28745]
- Cong WM, Bu H, Chen J, Dong H, Zhu YY, Feng LH; Guideline Committee. Practice guidelines for the pathological diagnosis of primary liver cancer: 2015 update. *World J Gastroenterol* 2016; **22**: 9279-9287 [PMID: 27895416 DOI: 10.3748/wjg.v22.i42.9279]
- Fan Y, Yu Y, Wang X, Hu M, Du M, Guo L, Sun S, Hu C. Texture Analysis Based on Gd-EOB-DTPA-Enhanced MRI for Identifying Vessels Encapsulating Tumor Clusters (VETC)-Positive Hepatocellular Carcinoma. *J Hepatocell Carcinoma* 2021; **8**: 349-359 [PMID: 33981636 DOI: 10.2147/JHC.S293755]

- 24 **Xia TY**, Zhou ZH, Meng XP, Zha JH, Yu Q, Wang WL, Song Y, Wang YC, Tang TY, Xu J, Zhang T, Long XY, Liang Y, Xiao WB, Ju SH. Predicting Microvascular Invasion in Hepatocellular Carcinoma Using CT-based Radiomics Model. *Radiology* 2023; **307**: e222729 [PMID: 37097141 DOI: 10.1148/radiol.222729]
- 25 **Zwanenburg A**, Vallières M, Abdalah MA, Aerts HJWL, Andrearczyk V, Apte A, Ashrafinia S, Bakas S, Beukinga RJ, Boellaard R, Bogowicz M, Boldrini L, Buvat I, Cook GJR, Davatzikos C, Depeursinge A, Desseroit MC, Dinapoli N, Dinh CV, Echegaray S, El Naqa I, Fedorov AY, Gatta R, Gillies RJ, Goh V, Götz M, Guckenberger M, Ha SM, Hatt M, Isensee F, Lambin P, Leger S, Leijenaar RTH, Lenkowitz J, Lippert F, Losnegård A, Maier-Hein KH, Morin O, Müller H, Napel S, Nioche C, Orlhac F, Pati S, Pfaehler EAG, Rahmim A, Rao AUK, Scherer J, Siddique MM, Sijtsema NM, Socarras Fernandez J, Spezi E, Steenbakkers RJHM, Tanadini-Lang S, Thorwarth D, Troost EGC, Upadhaya T, Valentini V, van Dijk LV, van Griethuysen J, van Velden FHP, Whybra P, Richter C, Lööck S. The Image Biomarker Standardization Initiative: Standardized Quantitative Radiomics for High-Throughput Image-based Phenotyping. *Radiology* 2020; **295**: 328-338 [PMID: 32154773 DOI: 10.1148/radiol.2020191145]
- 26 **Ding T**, Xu J, Zhang Y, Guo RP, Wu WC, Zhang SD, Qian CN, Zheng L. Endothelium-coated tumor clusters are associated with poor prognosis and micrometastasis of hepatocellular carcinoma after resection. *Cancer* 2011; **117**: 4878-4889 [PMID: 21480209 DOI: 10.1002/ncr.26137]
- 27 **Feng Z**, Li H, Zhao H, Jiang Y, Liu Q, Chen Q, Wang W, Rong P. Preoperative CT for Characterization of Aggressive Macrotrabecular-Massive Subtype and Vessels That Encapsulate Tumor Clusters Pattern in Hepatocellular Carcinoma. *Radiology* 2021; **300**: 219-229 [PMID: 33973839 DOI: 10.1148/radiol.2021203614]
- 28 **Kim KR**, Moon HE, Kim KW. Hypoxia-induced angiogenesis in human hepatocellular carcinoma. *J Mol Med (Berl)* 2002; **80**: 703-714 [PMID: 12436347 DOI: 10.1007/s00109-002-0380-0]
- 29 **Villa E**, Critelli R, Lei B, Marzocchi G, Cammà C, Giannelli G, Pontisso P, Cabibbo G, Enea M, Colopi S, Caporali C, Pollicino T, Milosa F, Karampatou A, Todesca P, Bertolini E, Maccio L, Martinez-Chantar ML, Turola E, Del Buono M, De Maria N, Ballestri S, Schepis F, Loria P, Enrico Gerunda G, Losi L, Cillo U. Neovascularization-related genes are hallmarks of fast-growing hepatocellular carcinomas and worst survival. Results from a prospective study. *Gut* 2016; **65**: 861-869 [PMID: 25666192 DOI: 10.1136/gutjnl-2014-308483]
- 30 **Dou TH**, Coroller TP, van Griethuysen JJM, Mak RH, Aerts HJWL. Peritumoral radiomics features predict distant metastasis in locally advanced NSCLC. *PLoS One* 2018; **13**: e0206108 [PMID: 30388114 DOI: 10.1371/journal.pone.0206108]
- 31 **Feng ST**, Jia Y, Liao B, Huang B, Zhou Q, Li X, Wei K, Chen L, Li B, Wang W, Chen S, He X, Wang H, Peng S, Chen ZB, Tang M, Chen Z, Hou Y, Peng Z, Kuang M. Preoperative prediction of microvascular invasion in hepatocellular cancer: a radiomics model using Gd-EOB-DTPA-enhanced MRI. *Eur Radiol* 2019; **29**: 4648-4659 [PMID: 30689032 DOI: 10.1007/s00330-018-5935-8]
- 32 **Önner H**, Abdülrezzak Ü, Tutuş A. Could the skewness and kurtosis texture parameters of lesions obtained from pretreatment Ga-68 DOTA-TATE PET/CT images predict receptor radionuclide therapy response in patients with gastroenteropancreatic neuroendocrine tumors? *Nucl Med Commun* 2020; **41**: 1034-1039 [PMID: 32516240 DOI: 10.1097/MNM.0000000000001231]
- 33 **Choi SY**, Kim SH, Park CK, Min JH, Lee JE, Choi YH, Lee BR. Imaging Features of Gadoteric Acid-enhanced and Diffusion-weighted MR Imaging for Identifying Cytokeratin 19-positive Hepatocellular Carcinoma: A Retrospective Observational Study. *Radiology* 2018; **286**: 897-908 [PMID: 29166246 DOI: 10.1148/radiol.2017162846]



Published by **Baishideng Publishing Group Inc**
7041 Koll Center Parkway, Suite 160, Pleasanton, CA 94566, USA

Telephone: +1-925-3991568

E-mail: office@baishideng.com

Help Desk: <https://www.f6publishing.com/helpdesk>

<https://www.wjgnet.com>

